Electronic Journal of Structural Engineering

eJSE INTERNATIONAL

Original Article

Cite this: DOI:10.56748/ejse.24617

Received Date:10 April 2024
Accepted Date:17 September2024

1443-9255
https://ejsei.com/ejse

Numerical simulation of mechanical properties and damage process of carbon nanotube concrete under triaxial compression and splitting conditions

Shanxiu Huang[a], Huikuan Li[a], Weijie Guo[a*], Jiaqi Guo[b], Xiaojiang Feng[c]

[a] School of Chemistry and Chemical Engineering, Henan Polytechnic University, Jiaozuo 454003, Henan, China
[b] School of Civil Engineering, Henan Polytechnic University, Jiaozuo 454003, Henan, China
[c] China Construction Seventh Bureau of Transportation Construction Co., LTD., Zhengzhou 450004, China
*Corresponding author: qwj900907@163.com

Abstract

To investigate the mechanical properties and failure processes of carbon nanotube concrete (CNTC), a three-dimensional meso-scale finite element model of concrete was constructed. Using ABAQUS software, numerical simulations were conducted on concrete samples with different carbon nanotube (CNT) concentrations under triaxial compression and splitting conditions. The results indicate that under splitting conditions, the failure of the specimens initially occurs along the loading direction from both ends, with few cracks and slow propagation. Subsequently, the cracks rapidly expand, penetrating the entire specimen, leading to the formation of a macro-fracture surface with a crack aligned with the loading direction. This failure mode manifests as a straight crack. At the same loading rate, the tensile strength of the specimens with different CNT concentrations increases to varying degrees during splitting failure, with a maximum increase of 45.10% to 4.15 MPa. U11nder triaxial compression conditions, the main failure mode of the specimens exhibits shear failure characteristics. As the confining pressure gradually increases, the failure angle of the specimens enlarges. Under low confining pressure, there are fewer wing-shaped tensile cracks at the shear failure surface of the specimens. As the confining pressure increases, irregular shear failures and multiple shear planes appear in the specimens, resulting in more complex failure modes. For specimens with the same CNT concentration, the triaxial compressive strength of CNTC specimens increases with increasing confining pressure. The triaxial compressive strengths of the specimens under confining pressures of 5 MPa, 10 MPa, 15 MPa, and 20 MPa are 90.48 MPa, 122.72 MPa, 137.22 MPa, and 172.65 MPa, with strength increases of 35.63%, 51.66%, and 90.81%, respectively.

Keywords

Carbon nanotubes, Concrete, Triaxial compression, Failure modes, Numerical simulation

1. Introduction

With the rapid development of the construction industry, the demand for improved performance of building materials is also increasing. Concrete, as the most used construction material in civil engineering infrastructure, has always been a research hotspot for performance optimization. Traditional concrete has significant limitations in tensile strength, deformation capacity, and crack resistance, which restricts its application in complex engineering environments (Liu et al. 2020). Therefore, how to further enhance the performance of concrete, not only to meet the basic bearing function but also to possess characteristics such as sustainability, intelligence, durability, multifunctionality, and high performance, has become an urgent problem to be solved. In recent years, the application of nanomaterials in concrete modification has attracted widespread attention. Among them, carbon nanotubes (CNTs), with their unique physical and chemical properties such as high strength, light weight, and high temperature resistance, have become an ideal choice for concrete reinforcement materials (Pitcha et al. 2022). Many scholars have attracted to incorporate CNTs into concrete to prepare modified carbon nanotube concrete (CNTC). Scholars at home and abroad have conducted extensive research on the mechanical properties of CNTC (Huang et al. 2023; Ma et al. 2014). Yin et al. (2021) found that when CNTs and steel fibers are simultaneously incorporated into concrete, their toughness and ductility are significantly improved compared to concrete with only steel fibers. The most significant enhancement in concrete performance occurs when the mixing proportions of steel fibers and CNTs are 1% and 0.30%, respectively. Yang et al. (2023) discovered that CNTs promote cement hydration through nucleation, increasing the amount of hydration product Ca (OH)2, and optimizing the pore structure and interfacial transition zone compactness of the material through filling and bridging effects, thereby optimizing the microstructure of cement-based materials. Tian et al. (2023) conducted split Hopkinson pressure bar (SHPB) impact tests and found that under impact loading conditions, the incorporation of CNTs alleviates the degree of concrete fracture, and its energy consumption, impact toughness, and dynamic strength are significantly improved. Jung et al. (2020) conducted uniaxial compression tests to investigate the influence of multi-wall CNT content on the compressive strength and deformation modulus of concrete. Sindu et al. (2017) performed uniaxial compression tests on concrete specimens with different CNT contents. The test results showed that the compressive strength of concrete specimens with a CNT content of 0.08% increased by 10%. Hamzaoui et al. (2012) studied the influence of CNT content on the compressive strength of concrete. The results showed that the compressive strength of concrete reached a maximum when the CNT content was 0.3%, an increase of 17.65% compared to plain concrete. Wang et al. (2013) measured the porosity and pore size distribution of CNTC using a mercury intrusion porosimeter. The results showed that the cement paste incorporated with CNTs has lower porosity and more uniform pore size distribution, with significant improvements in fracture energy and bending toughness index.

The research findings have greatly contributed to the development of CNTC in terms of mechanical properties, micro-mechanisms, and damage and failure mechanisms. However, current research on the mechanical properties of CNTC mainly focuses on the effect of CNT content on the strength and related performance parameters of concrete under uniaxial compression conditions (Marwan et al. 2022). There is a relative lack of research on the mechanical properties and failure processes of CNTC under splitting and triaxial compression conditions. Additionally, conducting indoor experiments on the failure process of CNTC under different conditions requires a significant amount of manpower, equipment, and time. Therefore, this study utilizes the ABAQUS finite element software to simulate the failure process of CNTC under splitting and triaxial compression conditions, avoiding the influence of dispersant dispersion effects on CNTC. The study analyzes the influence of CNT content and different confining pressures on the stress-strain curves, strength, and failure processes of concrete. The research findings are significant for the promotion and application of CNTC in practical engineering and the improvement of the stability and service performance of engineering structures.

2. Numerical simulation

2.1 Constitutive model of concrete damage evolution

Given that the tensile strength of concrete is significantly lower than its compressive strength, this study adopts the modified Mohr-Coulomb criterion and tensile criterion as the basis for judging the strength of element failure, with the tensile criterion having priority (Zhu et al. 2002; Lv et al. 2018). Once an element satisfies the tensile criterion, it will no longer be considered for the Mohr-Coulomb criterion. Damage begins to occur when the element reaches the tensile damage threshold. The damage variable caused by tensile stress is defined as follows:

$$D=\begin{cases}0, & \varepsilon_I<\varepsilon_{t0}\\ \left(1-\dfrac{\varepsilon_{t0}}{\varepsilon_I}\right)^n, & \varepsilon_{t0}\le\varepsilon_I\le\varepsilon_{tu}\\ 1, & \varepsilon_I\ge\varepsilon_{tu}\end{cases} \quad (1)$$

In the equation, E_I represent the maximum tensile principal strain, E_t0 is the threshold value of tensile damage strain, and E_"tu" is the ultimate tensile strain of the component.

The compressive damage is calculated using the modified Mohr-Coulomb criterion:

$$\varepsilon_I=\varepsilon_1-\varepsilon_3\frac{1+sin\varphi}{1-sin\varphi}\ge\varepsilon_{c0} \quad (2)$$

$$D=\begin{cases}0, & \varepsilon_I<\varepsilon_{c0}\\ \left(1-\dfrac{\varepsilon_{c0}}{\varepsilon_I}\right)^n, & \varepsilon_{c0}\le\varepsilon_I\le\varepsilon_{cu}\\ 1, & \varepsilon_I\ge\varepsilon_{cu}\end{cases} \quad (3)$$

In the equation, φ represents the internal friction angle, E_1 and E_3 are the maximum and minimum principal strains of the element, respectively, ε_I am the maximum principal compressive strain, and ε_ ("c" 0) is the compressive strain threshold of the component.

Based on the strain equivalence principle, the elastic modulus of a unit with an original elastic modulus of E after damage can be expressed as (1-D) E. After k iterations, the elastic modulus is calculated using the following formula:

$$E\left(1-D^{(k)}\right)=E\left(1-D^{(k-1)}\right)\left(1-D_{(k)}\right) \quad (4)$$

The damage evolution equation is:

$$D^{(k)}=1-\left[1-D^{(k-1)}\right]\left[1-D_{(k)}\right] \quad (5)$$

In the equation, Dk represents the cumulative damage of the element after iteration step k. D(k) is the damage generated in the kth step. The constitutive equation of the element at the kth step is:

$$\Delta\sigma_k=\left[1-D^{(k-1)}\right]\Delta\varepsilon_k \quad (6)$$

2.2 Material parameters and modeling

Concrete is a material composed of aggregates ranging from 5 to 20 mm mixed with cement mortar. The aggregate composition follows the Fuller grading curve and is randomly distributed within the cement matrix. Due to the differences in mechanical properties between the aggregates and mortar, combining them for detailed numerical simulation is crucial for a deep understanding of their mechanical behavior and failure mechanisms (Kormanikova et al. 2021). In the mesoscopic concrete model, the geometric shape and spatial distribution of aggregate directly affect the relative mechanical properties of concrete (Thilakarathna et al. 2020). The aggregates adopted in this paper are all gravel, with irregular polyhedral shapes. Assuming the aggregates are convex polyhedrons, each face of which is a triangle, the basic information of the aggregates, including the vertices of the convex polyhedrons and the topological relationship of the faces, is generated in MATLAB. The generation steps for a single aggregate are as follows: Randomly generate a radius value within the specified aggregate particle size range, reduce the spatial range of the sample inward, and randomly generate a point within this range. Randomly generate coordinates (,), and project them onto the spherical surface to obtain the first vertex V1. Use the same method to successively generate vertices V2 and V3, thereby obtaining the base triangle of the tetrahedron. To ensure that sphere center O is inside the random tetrahedron, randomly generate a point V4 within the range of the antipodal face of the triangular base and project it onto the spherical surface as the vertex of the random tetrahedron. At the same time, the other three faces F2, F3, and F4 of the tetrahedron can be obtained. Finally, perform face extension and edge extension of the polyhedron to obtain a random polyhedral aggregate with 17 vertices and 30 faces. (Wang et al. 2021). According to the mix ratio of poured concrete, the mass is converted to volume by density, and then the total aggregate is controlled by the aggregate volume ratio.

Monte Carlo method, also known as random sampling technique or peer testing method, utilizes random numbers to solve numerous computational problems (Dong et al. 2009). However, randomly generated aggregates may overlap in space. To determine whether a newly generated aggregate overlaps with the original ones, the following steps are adopted: (1) Initially screening out "suspicious" aggregates by conducting a preliminary discrimination on the sphere enclosing the polyhedral aggregate; (2) Narrowing down the range of "suspicious aggregates" through further discrimination based on the spatial relationship between vertices and faces; (3) Employing linear programming algorithms to conduct intersection discrimination on the "suspicious aggregates" to ensure no overlap occurs. Through these methods, a concrete model that meets the given aggregate grading can be constructed, as shown in Fig. 1 (a).

Table 1. Model material parameter

Constituent	Modulus of elasticity /GPa	Poisson ratio	ε_{t0}	ε_{c0}
Mortar	12.36	0.233	6.5×10^{-4}	5.3×10^{-3}
Aggregate	70.00	0.300	9.0×10^{-4}	5.3×10^{-3}

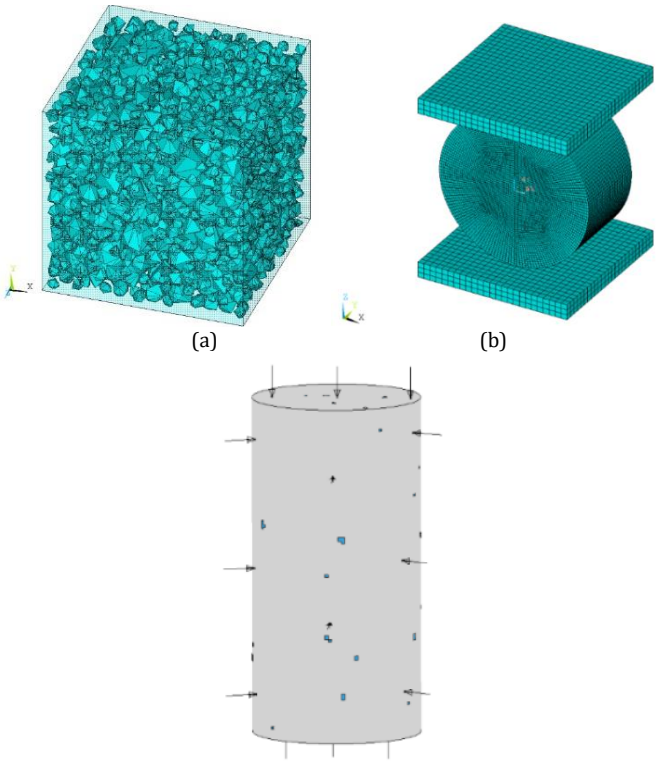

(a) (b) (c)

Fig. 1 3D meso-mechanical model of CNTC. (a) Random aggregate; (b) Splitting condition; (c) Triaxial compression

Treating CNT fibers and mortar matrix as a homogeneous material (Ji et al. 2024), the model parameters of CNTC after experimental calibration are shown in Table 1. The elastic moduli of the mortar matrix with different CNT dosages (0.05%, 0.1%, 0.3%, and 0.5%) are 14.38, 17.39, 16.64, and 13.76 GPa, respectively, and the Poisson's ratios are 0.239, 0.240, 0.239, and 0.221, respectively. The numerical model for the splitting experiment adopts a cylindrical cake-shaped sample with a diameter of 50 mm and a height of 25 mm, as shown in Fig. 1 (b). Based on fully characterizing the shape and size of the aggregate, a size of 0.625 mm is selected to ensure computational efficiency. During the experiment, both ends of the sample are fixed with rectangular steel plates and loaded axially at a rate of 1 kN/s, with a face-to-face erosion contact defined between them. The numerical model for the triaxial compression test includes a detailed concrete model and a pair of steel plates with a length and width of 70 mm and a thickness of 10 mm. The elastic modulus of the steel plates is taken as 210 GPa, and the upper and lower ends are loaded using steel plates. In the simulation, the end friction of the compressed sample can greatly affect its compressive strength and failure mode. Therefore, considering the end friction, a friction coefficient of 0.45 is taken, and the element size of the model is 2.5 mm. The simulation model of triaxial compression is shown in Fig. 1 (c).

3. Mechanical properties of CNTC

3.1 Numerical model validation

After curing the concrete samples for 28 days, the splitting tensile and triaxial compression tests were carried out according to the standard GB/T50081-2019, as shown in Fig. 2. The splitting tensile test results and simulation results are shown in Table 2, and the triaxial compression test results and simulation results at 10MPa confining pressure are shown in Table 3. The properties of concrete are affected by materials, test instruments and curing conditions. The experimental values of mechanical properties are somewhat discrete and differ from the numerical simulation results to some extent, but the maximum error between the test and numerical simulation is less than 9%, which proves the effectiveness of the three-dimensional mesoscopic model of CNTC.

(a) (b)

Fig. 2 Mechanical property test of CNTC. (a) Splitting tensile test; (b) Triaxial compression test

Table 2. Splitting tensile test results and simulation results

Dosage /%	Tensile strength /MPa				
	0	0.05	0.1	0.3	0.5
Experimental value	2.68	3.22	3.65	3.90	3.81
Simulated value	2.86	3.31	3.74	3.98	4.15

Table 3. Triaxial compression test results and simulation results

Dosage /%	Tensile strength /MPa				
	0	0.05	0.1	0.3	0.5
Experimental value	105.66	112.06	125.32	126.55	123.39
Simulated value	104.46	110.97	122.74	129.38	128.07

3.2 Mechanical properties of CNTC under splitting conditions

The splitting tensile stress-strain curves and tensile strengths of the samples with different CNT dosages are shown in Fig. 3. As shown in Fig. 3 (a), the stress-strain curves of concrete samples with different MWCNTs dosages exhibit similar trends during splitting failure under the same loading rate. With the increase of CNT dosage, the tensile strength of the samples is improved to varying degrees. Additionally, the incorporation of CNTs widens the "plateau region" at the peak stress of the concrete, indicating that CNTs enhance the toughness of the concrete to a certain extent, with the degree of improvement being related to the dosage of CNTs (Xia et al. 2021). According to Fig. 3 (b), when the dosages of CNTs are 0%, 0.05%, 0.1%, 0.3%, and 0.5%, the tensile strengths of the samples are 2.86 MPa, 3.31 MPa, 3.74 MPa, 3.98 MPa, and 4.15 MPa, respectively. Compared to the sample without CNTs, the tensile strengths increased by 15.73%, 30.77%, 39.16%, and 45.10%, respectively. Adding an appropriate amount of CNTs to concrete samples can effectively enhance their tensile strength. Furthermore, as the stress is applied to the samples, the transverse stress of the disks rapidly decreases after reaching the tensile strength, exhibiting obvious brittle fracture characteristics.

3.3 Mechanical properties of CNTC under triaxial compression conditions

As shown in Fig. 4, the stress-strain curves of the samples under different confining pressures successively undergo linear elastic deformation, nonlinear plastic deformation, and post-peak failure stages. With the same CNT dosage, the triaxial compressive strength of CNTC samples increase with the increase of confining pressure. Under confining pressures of 5 MPa, 10 MPa, 15 MPa, and 20 MPa, the triaxial compressive strengths of the samples are 90.48 MPa, 122.72 MPa, 137.22 MPa, and 172.65 MPa, respectively. Compared to the confining pressure of 5 MPa, the triaxial compressive strengths of the samples under confining pressures of 10 MPa, 15 MPa, and 20 MPa increase significantly by 35.63%, 51.66%, and 90.81%, respectively. This phenomenon occurs mainly because the strong confinement effect of high confining pressure inhibits the propagation of cracks in the CNTC samples, allowing them to fully utilize their strength. Additionally, with the increase of confining pressure, the CNTC samples exhibit significant ductility under triaxial stress. This is mainly due to the confining effect of the triaxial stress, which enables the CNTC to maintain a certain load-bearing capacity even after damage and failure, thereby ensuring a certain load-bearing capacity in the post-peak stage.

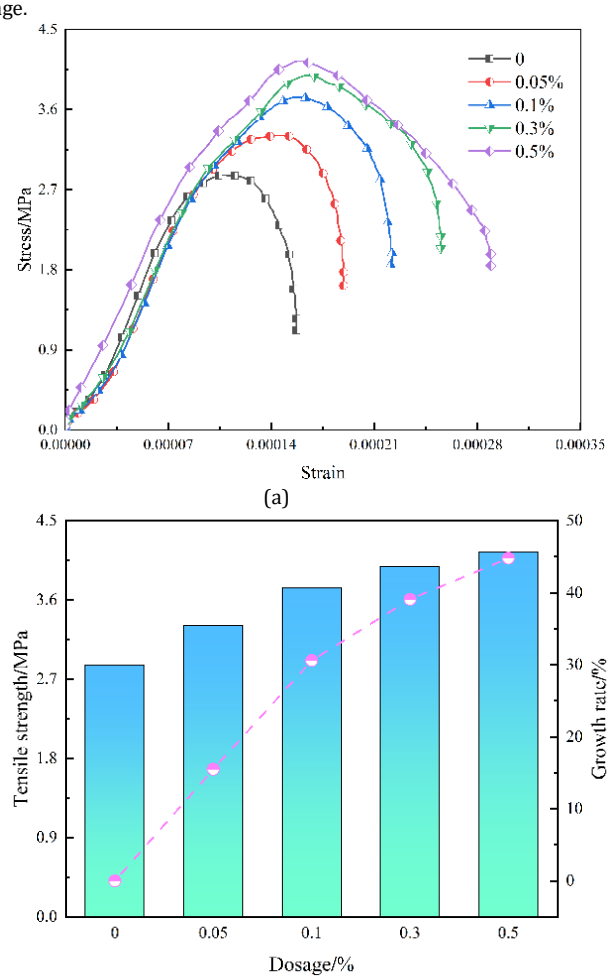

Fig. 3 Stress-strain curve and tensile strength of CNTC. (a) Stress-strain curve; (b) Tensile strength

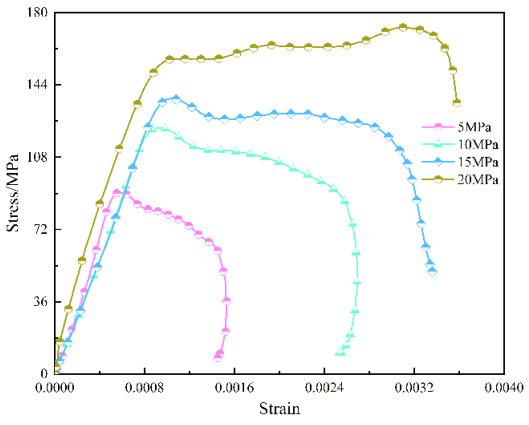

Fig. 5 displays the stress-strain curves of samples with different CNT dosages under a confining pressure of 10 MPa. As observed from the figure, the stress-strain curves of CNTC samples exhibit similar patterns under a confining pressure of 10 MPa, passing through the linear elastic deformation stage, plastic deformation stage, and ultimately the failure stage (Chen et al. 2020). During the elastic deformation stage, the strain-strain curve of the nanotube concrete samples exhibits a linear growth. As the axial loading continues to increase, irreversible plastic deformation begins to occur in the CNTC samples, and the degree of plastic deformation

intensifies with the increase in CNT dosage. Furthermore, the strength of the samples is also enhanced to varying degrees with the increase in CNT dosage. Specifically, when the CNT dosages are 0.05%, 0.1%, 0.3%, and 0.5%, the corresponding compressive strengths of the samples are 110.97 MPa, 122.74 MPa, 129.38 MPa, and 128.07 MPa, respectively. The compressive strength of concrete sample without CNTs is 104.46MPa, compared to the sample without CNTs, the strengths were improved by 6.23%, 17.50%, 23.86%, and 22.60%, respectively. This is consistent with the results of Huang's study (Huang. 2022). Although the compressive strength of the samples generally increases with the increase in CNT dosage, a slight decline in compressive strength is observed when the CNT dosage exceeds 0.3%. Therefore, to ensure the compressive strength of the samples, it is crucial to control the dosage of CNTs within a certain range.

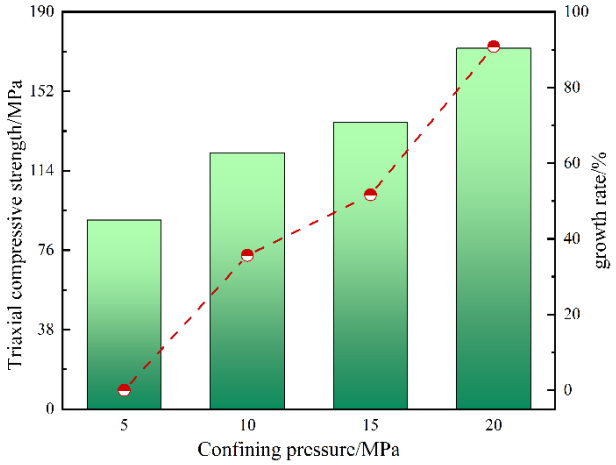

Fig. 4 Stress-strain curve and triaxial compressive strength of concrete under different confining pressures. (a) Stress-strain curve; (b) Triaxial compressive strength

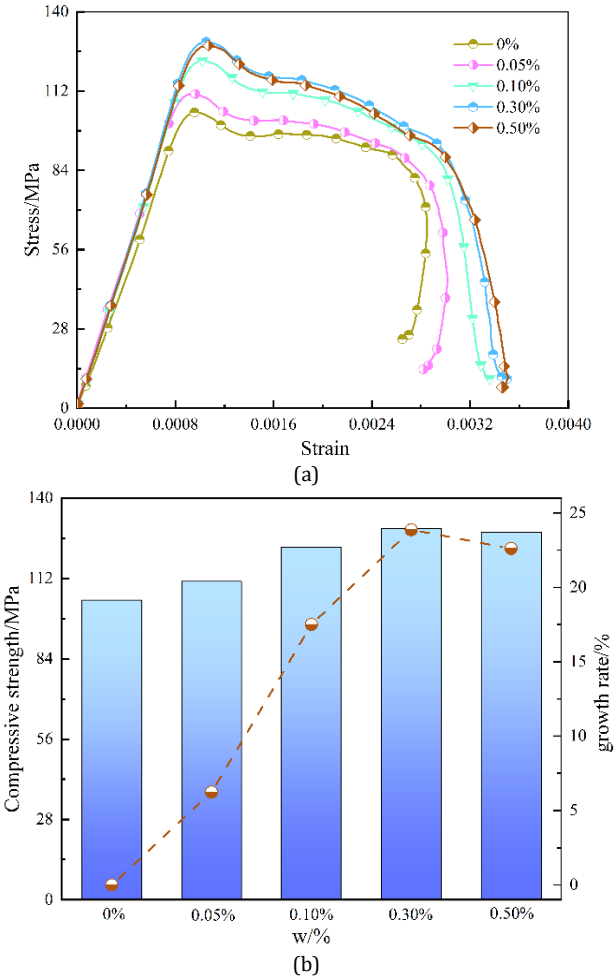

Fig. 5 Stress-strain curve and triaxial compressive strength of concrete with different CNTs content. (a) Stress-strain curve; (b) Triaxial compressive strength

4. CNTC destruction process

4.1 Destruction process of CNTC under splitting conditions

Strain field evolution process

Taking the sample with a CNT doping content of 0.1% as an example, we analyze the evolution process of the internal strain field under splitting conditions. As shown in Fig. 6, along the direction of the primary stress loading, stress concentration first occurs at the upper and lower ends of the sample. Large displacements appear at the interaction points with the loading plates, indicating that the surface of the sample in these areas has been compressed and yielded. As the loading continues, the sample sustains continuous compression in the vertical direction. Cracks initiate at the ends and gradually propagate towards the central axis, along the mortar transition interface between the coarse aggregate and the cement matrix. Microcracks accumulate and gradually expand under tensile stress. With the further increase of the load, the displacement of the particles increases, and the tensile stress parallel to the primary stress becomes larger, leading to new stress concentrations at the crack tips. This causes the cracks to propagate further until they connect from the top to the bottom of the sample, resulting in instability. Simultaneously, near the two endpoints of the disk perpendicular to the loading direction, a significant distribution of tensile stress can also be observed. These are the locations where tensile failure occurs, and initial cracks first appear. Along the loading axis, the stress distribution is uneven, and the instability mode is characterized as splitting failure.

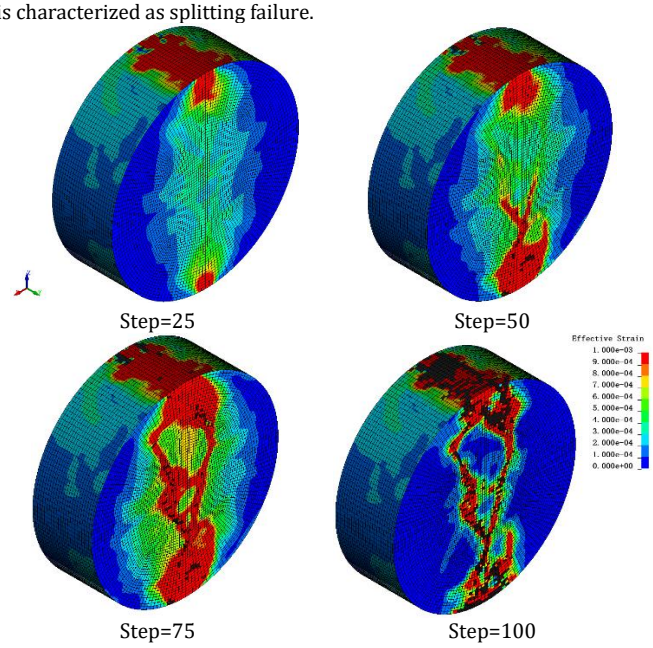

Fig. 6 Evolution of equivalent strain cloud diagram

Destruction process under cleavage conditions

An analysis of the failure morphology of the sample with a CNT doping content of 0.1% is conducted, as shown in Fig. 7. Initially, during loading, the disk cracks initiate from both ends along the loading direction, with few cracks and slow propagation. As the sample enters the unstable rupture development stage, the cracks develop rapidly, and the elastic strain energy is quickly released, driving the cracks to expand rapidly and penetrate the entire specimen. Subsequently, a macroscopic fracture surface forms, resulting in a crack aligned with the loading direction. The failure mode exhibits a straight crack, and the final crack formed basically overlaps with the loading centerline of the specimen. It can be observed that the main crack leading to the ultimate failure is not caused by the central crack of the specimen but rather originates from the destruction of the two end faces. As the displacement load gradually increases, the crack gradually extends towards the central position along the axis, ultimately forming a through-crack that destroys the sample.

Destruction pattern under cleavage conditions

As shown in Fig. 8, the failure morphologies of concrete samples with different CNT doping contents exhibit significant differences. Firstly, when the doping content of CNTs in the sample is low, the failure process is typically characterized by the appearance of a crack in the center of the end face, which gradually expands and penetrates the entire sample. However, as the doping content of CNTs increases, the failure morphology undergoes certain changes. At this point, the failure of the sample is more often caused by the expansion of microcracks parallel to the direction of the main stress, forming a main crack that gradually enlarges and

ultimately leads to the failure of the sample. Notably, with the increase in CNT doping content, the number of cracks produced during the final failure of the sample decreases significantly. This phenomenon indicates that the addition of CNTs has a positive impact on the tensile strength of the concrete sample. As a nanomaterial with excellent mechanical properties, CNTs can effectively improve the microstructure of concrete, enhance the internal bonding force within the concrete, and thereby increase the tensile strength of the sample. Therefore, as the doping content of CNTs increases, the sample can better resist failure when subjected to external forces, resulting in a corresponding decrease in the number of cracks.

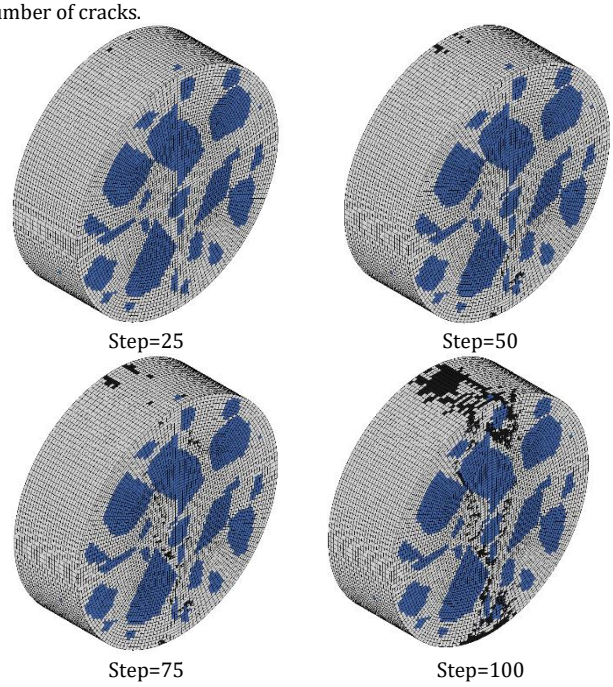

Fig. 7 Graphical representation of the splitting damage process

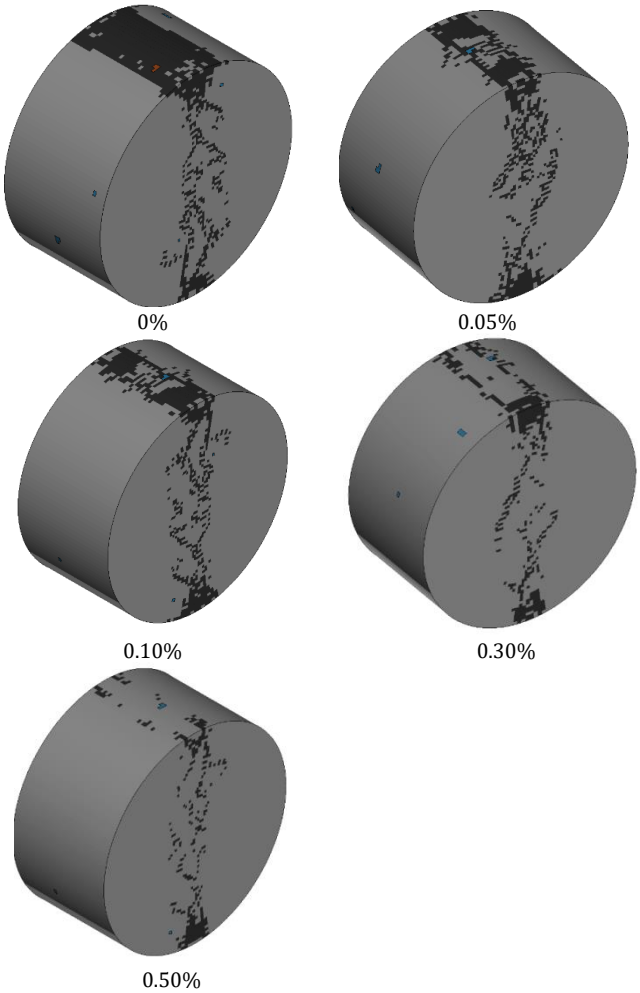

Fig. 8 Failure modes of samples with different CNT content

4.2 Destruction process of CNTC under triaxial compression conditions

Strain field evolution process

In Fig. 9, the loading process of the sample, as well as the subtle changes in its internal displacement field and crack propagation, can be observed in detail. During the initial stage of loading, the displacement field within the sample exhibits a relatively uniform distribution. At this point, the displacement borne by the aggregate within the sample is relatively small, indicating that the overall structure of the sample is still in a relatively stable state during the initial loading phase. As loading gradually begins, tiny cracks start to appear at the mortar transition interfaces on the top and inside of the sample. These cracks mark the initial damage to the sample. Although the cracks are small and few at this point, they have already had an impact on the structural integrity of the sample. However, even in this state of initial damage, the overall displacement field distribution within the sample remains relatively uniform, indicating that the sample still possesses a certain degree of load-bearing capacity during the initial stage. As loading continues, the cracks within the sample begin to propagate and extend along the mortar transition interfaces between the coarse aggregate and the cement matrix, and the number of cracks further increases. Significant local deformation and displacement have occurred within the sample, indicating a worsening degree of damage. Ultimately, under continuous loading, the cracks within the sample propagate and penetrate the entire sample, resulting in significant displacement and deformation. The sample loses its load-bearing capacity and fails.

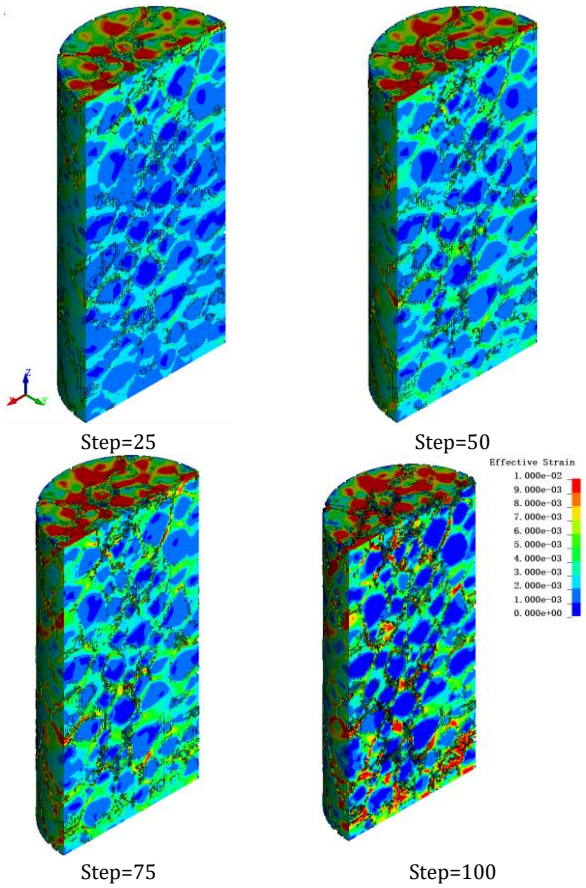

Fig. 9 Evolution of equivalent strain cloud diagram

Triaxial compression damage process

Taking the sample with a CNT doping content of 0.1% under a confining pressure of 15 MPa as an example, its failure process under triaxial compression is analyzed. As shown in Fig. 10, when subjected to triaxial confining pressure, microcracks first appear at the upper and lower end faces of the sample, which are the most concentrated areas of stress. The emergence of these microcracks is caused by the uneven distribution of internal stress in the sample under external pressure, resulting in stress concentration in local areas. Meanwhile, a small number of cracks are also observed at the mortar transition interfaces between the coarse aggregate and the cement matrix within the sample. This is due to the difference in mechanical properties between the coarse aggregate and the cement matrix. When subjected to external pressure, this difference leads to stress concentration at the interfaces, triggering the formation of cracks. As the pressure gradually increases, these microcracks begin to develop continuously. In this process, the distance between the coarse aggregates is further compressed, as the overall volume of the sample

shrinks under pressure, resulting in a reduction in the spacing between the coarse aggregates. As the loading process continues, the microcracks start to propagate and extend along the mortar transition interfaces. The propagation paths of these cracks are often influenced by the distribution of the coarse aggregate and the characteristics of the mortar transition interfaces, exhibiting a complex network-like structure. Eventually, when the cracks propagate to a certain extent, they interconnect, forming a crack network that penetrates the entire sample. At this point, the sample is unable to bear any further external pressure and fails.

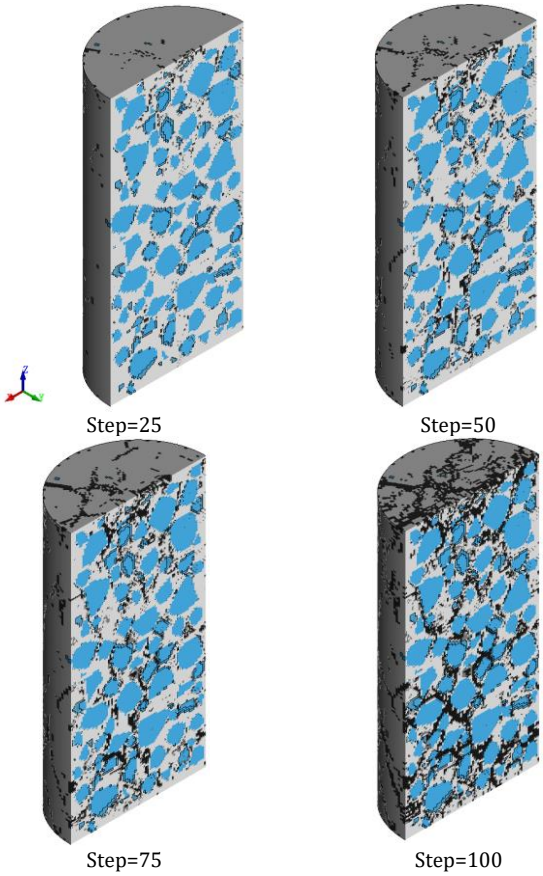

Fig. 10 Failure process under triaxial compression

Triaxial compression damage pattern

The failure modes of concrete samples with different CNT doping levels (0, 0.05%, 0.1%, 0.3%, and 0.5%) loaded to unloading under various confining pressures (5 MPa, 10 MPa, 15 MPa, and 20 MPa) are shown in Figure 11. The triaxial loading process of the samples until their failure involves the following stages: elastic deformation, crack initiation and propagation, and unstable crack propagation leading to failure. Under triaxial compression, the main failure mode of the samples exhibits shear failure characteristics. It is generally believed that the failure form of the samples is caused by the end effect (the frictional constraint effect between the two end faces of the sample and the loading platen). Different friction forces between the two end faces of the sample and the loading platen result in different failure modes. Additionally, the failure modes of the samples also vary due to different CNT doping levels and confining pressures. Therefore, the failure mode of the specimens is influenced by multiple factors. The impact of confining pressure on the strength of the samples is significant. As seen in the figure, as the triaxial confining pressure increases, the number of cracks resulting from the failure damage decreases, indicating that the triaxial compressive strength of the samples increases with the increase in confining pressure. Simultaneously, as the confining pressure gradually increases, the failure angle of the sample also increases. Under low confining pressures, the wing-shaped tensile cracks at the shear failure surface of the 5 MPa specimens are relatively few. As the confining pressure increases, the rock specimens under 10 MPa exhibit irregular shear failure with multiple shear planes, and the failure mode of the specimens tends to become more complex. However, the failure modes of samples with different CNT doping levels under the same confining pressure are roughly the same, primarily exhibiting shear failure, and the failure of the samples is more pronounced under low confining pressures (around 5 MPa).

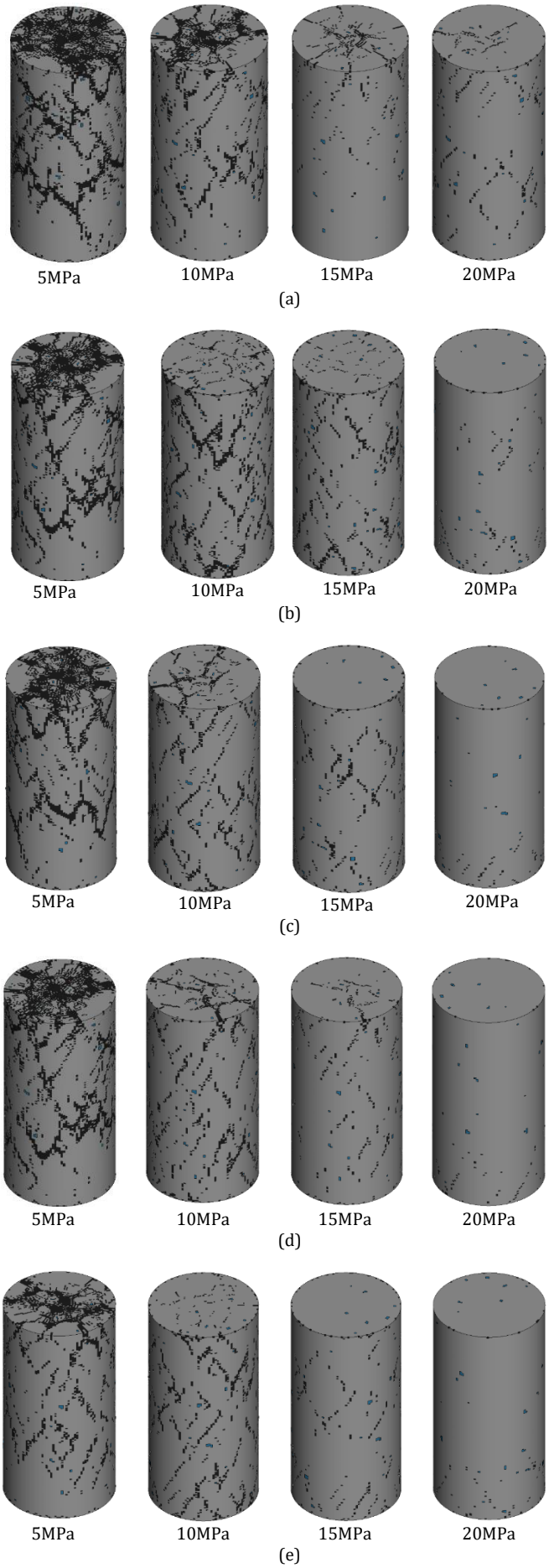

Fig. 11 Failure modes of the samples under different CNT dosage and confining pressure conditions. (a) 0%; (b) 0.05%; (c) 0.10%; (d) 0.30%; (e) 0.50%

5. Conclusion

Using the ABAQUS finite element software, this paper established numerical models of concrete with various CNT doping levels to simulate the progressive failure process of CNTC specimens under triaxial compression and splitting conditions. By analyzing the mechanical properties and failure processes of the specimens under different CNT doping levels and confining pressures, the following conclusions were drawn:

1. Under splitting conditions, the ultimate failure of the specimen is caused by the through-cracking of the central fissure on the end face or the formation of a main crack parallel to the principal stress direction through the connection of micro-cracks generated in parallel with the principal stress. The instability mode is splitting failure. With the same loading rate, the tensile strength of the specimen can be increased by a maximum of 45.10% to 4.15 MPa as the doping level of CNTs increases.
2. The stress-strain curves of CNTC specimens under different confining pressures all undergo linear elastic deformation, nonlinear plastic deformation, and post-peak failure stages. The triaxial compressive strength of CNTC specimens increases with the increase in confining pressure. As the confining pressure increases, the CNTC specimens exhibit significant ductility under triaxial stress.
3. Under triaxial compression conditions, the main failure mode of the specimen exhibits shear failure characteristics. Additionally, the failure of the specimen is more evident under low confining pressures (around 5 MPa). Under the same confining pressure, when the doping level of CNTs is 0.3%, the corresponding compressive strength of the specimen is 129.38 MPa, representing the maximum strength enhancement of 23.86% compared to the specimen without CNTs. Under the same doping level of CNTs, the compressive strength of the specimen reaches a maximum of 172.65 MPa under a confining pressure of 20 MPa, representing an increase of 90.81%.

Acknowledgments

This study was funded by projects such as National Natural Science Foundation of China (Grant No. 52178388); Enterprise commissioned project (Grant No. H22-661).

Disclosure statement

The authors declare that they have no conflicts of interest.

References

Liu QL, Li HC, Peng YJ, Dong XB. 2020. Nanomechanical properties of multi-wall carbon nanotubes/cementitious composites. Acta Materiae Compositae Sinica, 37(4): 952–961.

Pitcha J, Chanachai T, Amaras M, Tosporn P, Musa A, Shanya A. 2022. Enhancing bonding behavior between carbon fiber-reinforced polymer plates and concrete using carbon nanotube reinforced epoxy composites. Case Studies in Construction Materials, 17: e01407.

Huang SX, Cheng XY, Zhang CX, Guo JQ. 2023. Mechanical Properties and Energy Evolution Characteristics of Concrete under Different Strain Rates and Content of MWCNTs. Chinese Journal of High-Pressure Physics, 37(01): 44-53.

Ma Y, Wang D, Wang Q. 2014. Preparation of multi-wall carbon nanotubes renforced cement composites and study of their mechanical properties. Concrete, 06: 72-74+77.

Yin P, Sun M, Dong ZS. 2021. Influence of carbon nanotubes and steel fiber on compressive strength and impact resistance of concrete. China Concrete and Cement Products, 03:52-55.

Yang ZQ, Zhu HL. 2023. Study on the effect of carbon nanotubes on the microstructure and anti-carbonation properties of cement-based materials. Journal of Functional Materials, 54(08):8217-8227.

Tian W, Gao FF. 2023. A study on fracture fractal of high temperature spray cooled carbon nanotube concrete under impact load. Journal of Vibration and Shock, 42(04): 71-80.

Jung M, Lee Y, Hong S, Moon J. 2020. CNTs (CNTs) in ultra-high-performance concrete (UHPC): Dispersion, mechanical properties, and electromagnetic interference (EMI) shielding effectiveness (SE). Cement and Concrete Research, 131 106017.

Sindu B, Sasmal S. 2017. Properties of carbon nanotube reinforced cement composite synthesized using different types of surfactants. Construction and Building Materials, 155: 389-399.

Hamzaoui R, Bennabi A, Guessasma S, Khelifa MR, Leklou N. 2012. Optimal Carbon Nanotubes Concentration Incorporated in Mortar and Concrete. Advanced Materials Research, 2046(587): 107-110.

Wang B, Han Y, Liu S. 2013. Effect of highly dispersed carbon nanotubes on the flexural toughness of cement-based composites. Construction and Building Materials, 46: 8-12.

Marwan HA, Muyideen A, Jassam MT, Mansob RA. 2022. Mechanical properties of concrete containing recycled concrete aggregates and multi-walled carbon nanotubes under static and dynamic stresses. Case Studies in Construction Materials, 17: e01651.

Zhu WC, Tang CA, Zhao W, Teng JG. 2002. Numerical simulation on the fracture process of concrete specimen under static loading. Engineering Mechanics, 19: 148-153.

Lv T, Chen X, Chen G. 2018. The 3D meso-scale model and numerical tests of split Hopkinson pressure bar of concrete specimen. Construction and Building Materials, 160: 744-764.

Kormanikova E, Zmindak M, Novak P, Sabol P. 2021. Tensile properties of carbon fiber reinforced polymer matrix composites: Application for the strengthening of reinforced concrete structure. Composite Structures, 275: 114448.

Thilakarathna P, Baduge KK, Mendis P, Vimonsatit V, Lee H. 2020. Mesoscale modelling of concrete – A review of geometry generation, placing algorithms, constitutive relations and applications. Engineering Fracture Mechanics, 231:106974.

Wang SR, Zhao JQ, Wu XG. 2021. Meso-Scale Simulations of Lightweight Aggregate Concrete under Impact Loading. International Journal of Simulation Modelling, 20(2):291-302.

Dong YQ, Zhang XH. 2009. Analysis on Structure Reliability with Monte Carlo Finite Element Method. Forest Engineering, 25(05): 73-75+88.

Ji YC, Wang DY Jia YM. 2025. Numerical Simulation and Size Effect Study on PVA Fiber-reinforced Brick Aggregate Recycled Concrete. Materials Reports, 39(3): 23100214.

Xia W, Xu JY, Nie XL. 2021. Dynamic Compressive Mechanical Properties of Carbon Nanofibers Reinforced Concrete under lmpact Loading. Materials Reports, 35(22): 22063-22071.

Chen L, Zhang X, Liu G. 2020. Analysis of dynamic mechanical properties of sprayed fiber-reinforced concrete based on the energy conversion principle. Construction and Building Materials, 254: 119167.

Huang SX. 2023. Research on mechanical-electronic properties and self-repairing mechanism of carbon nanotubes-reinforced concrete. Henan Polytechnic University, 1-171

Disclaimer